© 2023 Journal of Pharmacy & Pharmacognosy Research, 11 (5), 810-822, 2023
ISSN 0719-4250
https://jppres.com

DOI: https://doi.org/10.56499/jppres23.1688_11.5.810

Original Article

Lead compound discovery using pharmacophore-based models of small-molecule metabolites from human blood as inhibitor cellular entry of SARS-CoV-2

[Descubrimiento de compuestos principales utilizando modelos farmacóforos de metabolitos de moléculas pequeñas procedentes de sangre humana como inhibidores de la entrada celular del SARS-CoV-2]

Ellin Febrina[1*], Aiyi Asnawi[2]

[1]Faculty of Pharmacy, Universitas Padjadjaran, Jl. Raya Bandung-Sumedang Km. 21, Jatinangor, Sumedang, West Java, 45363, Indonesia.
[2]Faculty of Pharmacy, Universitas Bhakti Kencana, Jl. Soekarno Hatta No.754, Bandung, West Java, 40617, Indonesia.
*E-mail: ellin.febrina@unpad.ac.id

Abstract

Context: The development of emerging viral diseases like SARS-CoV-2 has underlined the critical need for new antiviral medicines. Many of the discovered inhibitors have off-target effects or toxicity issues, but no single lead chemical has been found as a powerful SARS-CoV-2 inhibitor. Small-molecule metabolites from human blood, for example, have been demonstrated to exhibit biological action, such as anti-inflammatory or antiviral properties, but have not been reported as pharmacophore-based drug discovery models.

Aims: To evaluate the feasibility of employing pharmacophore models of small-molecule metabolites taken from human blood as a lead discovery method for SARS-CoV-2 inhibitors.

Methods: A total of six small-molecule metabolites from human blood were utilized to construct a pharmacophore model, which was then used to simulate the interaction's stability for the top two-rank ligands with the best interactions using molecular docking and molecular dynamics.

Results: The area under the curve value of the pharmacophore model created using the best pairwise alignments approach was 0.576, indicating that it is suitably validated as a model. The pharmacophore model was utilized for virtual screening, followed by molecular docking, yielding 75 hits. An investigation of the molecular dynamics of two top-rank hits (ZINC000085567845 and ZINC000085567870) revealed a stable interaction with the SARS-CoV-2 spike protein.

Conclusions: Finally, the pharmacophore model developed was capable of discovering lead compounds with the potential as SARS-CoV-2 spike protein inhibitors.

Keywords: antiviral; molecular docking; molecular dynamics; SARS-CoV-2; screening.

Resumen

Contexto: El desarrollo de enfermedades víricas emergentes como el SARS-CoV-2 ha subrayado la necesidad crítica de nuevos medicamentos antivirales. Muchos de los inhibidores descubiertos tienen efectos fuera de diana o problemas de toxicidad, pero no se ha encontrado ninguna sustancia química líder que sea un potente inhibidor del SARS-CoV-2. Se ha demostrado, por ejemplo, que los metabolitos de moléculas pequeñas de la sangre humana presentan una acción biológica, como propiedades antiinflamatorias o antivirales, pero no se ha informado de ellos como modelos de descubrimiento de fármacos basados en farmacóforos.

Objetivos: Evaluar la viabilidad de emplear modelos farmacóforos de metabolitos de moléculas pequeñas extraídos de la sangre humana como método de descubrimiento de inhibidores del SARS-CoV-2.

Métodos: Se utilizó un total de seis metabolitos de moléculas pequeñas de sangre humana para construir un modelo farmacóforo, que luego se utilizó para simular la estabilidad de la interacción para los ligandos de dos rangos superiores con las mejores interacciones utilizando acoplamiento molecular y dinámica molecular.

Resultados: El valor de área bajo la curva del modelo farmacóforo creado mediante el enfoque de los mejores alineamientos por pares fue de 0,576, lo que indica que está adecuadamente validado como modelo. El modelo farmacóforo se utilizó para el cribado virtual, seguido del acoplamiento molecular, con 75 resultados. Una investigación de la dinámica molecular de dos de los hits de mayor rango (ZINC000085567845 y ZINC000085567870) reveló una interacción estable con la proteína espiga del SARS-CoV-2.

Conclusiones: Finalmente, el modelo farmacóforo desarrollado fue capaz de descubrir compuestos líderes con potencial como inhibidores de la proteína espiga del SARS-CoV-2.

Palabras Clave: acoplamiento molecular; antiviral; cribado; dinámica molecular; SARS-CoV-2.

ARTICLE INFO
Received: May 16, 2023.
Accepted: August 12, 2023.
Available Online: September 6, 2023.

AUTHOR INFO
ORCID:
0000-0003-3004-5069 (EF)
0000-0002-8179-0520 (AA)

INTRODUCTION

The coronavirus disease 2019 (COVID-19) outbreak, caused by the severe acute respiratory syndrome coronavirus 2 (SARS-CoV-2) has turned into a global health crisis (La Torre et al., 2020; Mayer et al., 2019). Despite the availability of vaccines, the continuing appearance of novel variants and the possibility for viral alterations underline the need for effective treatments to battle the ongoing pandemic (Zhou et al., 2020). One possible option is the creation of small-molecule inhibitors of SARS-CoV-2 entrance into host cells, a critical step in the viral life cycle (Li and De Clercq, 2020).

Despite the rapid development of COVID-19 vaccines (Krammer, 2020), there is still an urgent need for effective SARS-CoV-2 treatments. One intriguing strategy is to create small-molecule inhibitors that can prevent the virus from entering the cell via the interaction between the viral spike protein and the human ACE2 receptor. While multiple small-molecule inhibitors have been found using various screening approaches, we still have a huge gap in our understanding of the molecular processes behind viral binding and inhibition (Ndwandwe and Wiysonge, 2021).

There is currently no one lead molecule that has been identified as a potent SARS-CoV-2 inhibitor (Liu et al., 2020). The bulk of the discovered inhibitors are either in the early stages of development or have demonstrated poor efficacy in clinical trials. Furthermore, many of the identified inhibitors have been shown to have off-target effects or toxicity concerns, emphasizing the importance of further optimizing and refining these compounds (Citarella et al., 2021). One potential method to solve this research gap is to apply pharmacophore-based models of small-molecule metabolites from human blood as a starting point for inhibitor development (Jackson et al., 2022). These models can be developed based on known small-molecule metabolites that have been shown to have biological activity, such as anti-inflammatory or antiviral characteristics. Using these models, researchers can find drugs with similar structural and functional properties that may successfully prevent the interaction between the viral spike protein and the human ACE2 receptor.

To the best of our knowledge, there has been little study on the use of pharmacophore-based models for lead drug identification against SARS-CoV-2 (El-Ashrey et al., 2022). As a result, there is a substantial research gap in this field, which the current work attempts to solve by constructing and employing such models to identify new SARS-CoV-2 small-molecule inhibitors. We expect that by doing so, we can help the development of effective COVID-19 therapeutics as well as provide insights into the molecular mechanisms of virus entrance and suppression.

In drug discovery, pharmacophore-based models have been frequently utilized to find and optimize lead compounds with high affinity for target proteins. The goal of this study was to employ pharmacophore-based models using small-molecule metabolites from human blood to find a potential lead drug from a library natural product to prevent SARS-CoV-2 cellular entrance. These metabolites have been demonstrated to have a wide variety of biological actions and are easily tested.

The pharmacophore-based models were created using the best pairwise alignments (BPA) method, which is a well-known and established method for creating accurate pharmacophore models. The models were built using structural features of known inhibitors of SARS-CoV-2 entry as well as existing knowledge about viral entry mechanisms. The generated pharmacophore models were then utilized to screen a library of natural product small molecules, yielding a list of probable hits.

The virtual screening hits were confirmed further using molecular docking as well as molecular dynamics simulations to determine their binding affinities and modalities of interaction with the SARS-CoV-2 spike protein receptor-binding domain (RBD). The RBD is the primary protein domain that facilitates the virus's contact with host cell receptors. As a result, hits with high binding affinities and unique mechanisms of interaction with the RBD may be able to prevent viral entrance into host cells.

Overall, this study aimed to show the potential of using pharmacophore models of small-molecule metabolites derived from human blood as a tool for lead drug discovery in the quest for SARS-CoV-2 entrance inhibitors. The findings of this work could contribute to the development of novel COVID-19 therapies by providing insights into the potential pharmacological effects of small-molecule metabolites.

MATERIAL AND METHODS

Hardware

The hardware used was a Server HP Z820 WorkStation with the following specifications: an Intel Xeon E5-2667 Double Processor, a Nvidia® GTX 970 graphics processing unit (GPU), 32 GB of random-access memory (RAM), and a dual system running Ubuntu 20.04 LTS and Windows 10 Pro-64-bit for

Table 1. Training set (Tong et al., 2022) and best pairwise solution of a pharmacophore model.

Training set	IC_{50} (μM)	Best pairwise alignments
1,5-Anhydro-D-sorbitol	27.44	
1-Naphthol	9.77	
4-Hydroxyretinoic acid	7.18	
5-Methoxytryptophol	43.10	
Chenodeoxycholic acid	9.68	
Ellagic acid	13.00	

molecular docking and molecular dynamics simulations.

Preparation of training set, active dataset, and decoy

The training set used as many as 6 active compounds (see Table 1) (Tong et al., 2022). The 30 active compounds as active datasets were retrieved from the ChEMBL database (Gaulton et al., 2017), which had been examined as having potential value experimentally against SarCov2 targets. The decoys dataset was generated by using DecoyFinder 2.0 (Adrià et al., 2012) to generate structurally similar compounds to active compounds but with different chemical properties. The 3D structure of these datasets was downloaded in *.sdf format from the PubChem substance and compound databases (Kim et al., 2019).

Preparation of 3D crystal structure for the SARS-CoV-2 main protease

The 3D crystal structure of the SARS-CoV-2 main protease protein (PDB ID 7BQY) was downloaded from the RCSB Protein Data Bank (PDB) (https://pubchem.ncbi.nlm.nih.gov/) in *.pdb. With the Discovery Studio 2016 application (Jejurikar and Rohane, 2021), the native ligand, water molecules, solvents, and other non-standard residues are taken out of this structure. The addition of polar hydrogen atoms and charge of the protein was done using AutoDockTools 1.5.6 (Febrina et al. 2022; Huey et al. 2012).

Pharmacophore model analysis

The training set was used to generate pharmacophore models by using PharmaGist (Schneidman-Duhovny et al., 2008). The model's performance was assessed using metrics such as accuracy, sensitivity, specificity, and the area under the curve (AUC) of the receiver operating characteristic (ROC) curve. Validation of the pharmacophore model was carried out website-based (Empereur-Mot et al., 2016) to detect the best model with an AUC value criterion of ROC of more than 0.5.

Database screening

The ZINC15 database was queried to retrieve 270,547 natural product chemicals that were chosen as library databases (Sterling and Irwin, 2015). The screening of database compounds was carried out using PharmaGist based on the best-based pharmacophore model obtained from the pharmacophore model analysis stage. The database screening results were defined as hits compounds from pharmacophore-based screening.

Molecular docking simulation

The screening process was continued using molecular docking simulation via the Autodock wizard program of PyRx (Dallakyan and Olson, 2015). Hits of pharmacophore-based screening were docked to the validated 7BQY active site. Other criteria used include rigid protein, genetic algorithm parameters with GA RUN = 20, and maximum number of evaluations = 25,000,000 on the number of twistable bonds. The free energy of binding native ligands was used as a reference in determining hits from docking-based screening. Interpretation of molecular docking result including the free energy of energy (ΔG), inhibition constant (Ki), and the ligand interaction with amino acid residues of the active site.

Molecular dynamics simulation

The two best hits from docking-based screening and native ligand (positive control) were continued to the molecular dynamics simulation stage. Molecular dynamics simulations were carried out using the GROMACS program (Kutzner et al., 2022). Protein topologies were prepared using AMBER99SBILDN produced by Gromacs, and ligand topologies were prepared using General AMBER Force Field (GAFF) (He et al., 2020) generated using the Antechamber program package from Ambertools 2021 (Case et al., 2021) with the help of Acpype (Bernardi et al., 2019). In the MD simulation, the initial conformation of the protein-ligand complex was derived from the docking simulation of the molecule with the lowest binding

energy. This complex exists in the aqueous environment in the form of a cubic box using the TIP3P water molecule model (Mark and Nilsson, 2001). A neutral system is obtained after the addition of Na+/Cl- ions. An equilibrium system consisting of proteins, ions, and ligands was obtained after simulating NVT and NPT at 310 K 100 ps each. The production system takes place at a temperature of 310 K and a pressure of 1 bar for 100 ns. The molecular dynamics simulation stage includes several stages (for more details, please follow (Asnawi et al. 2023; Febrina et al. 2022). The simulation results were analyzed using root mean square deviation (RMSD) and root mean square fluctuation (RMSF) values, and the binding free energy was calculated using the molecular mechanics generalized born surface area (MMGBSA) approach (Genheden and Ryde, 2015).

Data analysis

The analysis of the data was obtained for ligand-based virtual screening, which involved scoring functions based on pharmacophore patterns. The similarity analysis was used to identify compounds that share similar features with known active compounds and are more likely to be active. Validate the docking protocol by redocking the cocrystallized ligand (the native ligand) and figuring out the RMSD between the predicted and experimental binding modes (less than 2). The generated poses or binding modes were evaluated and analyzed after the docking simulation. When the poses were compared to those of the native ligand, they were judged on how well they could choose good binding poses for each ligand and rank the ligand library to find hits with high scores. Scoring functions were used to estimate the binding affinities or energy values of the ligand-protein interactions. All data were processed and displayed in tables and figures. The data obtained from molecular dynamics simulations can be analyzed in various ways to gain insights into the behavior and properties of macromolecules, such as RMSD, RMSF, and MMGBSA.

RESULTS

In silico drug design methods are emerging as an important tool to design novel proteins or drugs in the fields of biotechnology and pharmaceutical drug development. These bioinformatics methods have been of great importance in the target identification and prediction of novel drugs against various human diseases (Ritchie and McLay, 2012). Thus, the present study attempted to evaluate the pharmacophore model from small-molecule metabolites from human blood in screening library natural products to obtain the potential lead compound as an inhibitor for SARS-CoV-2.

Pharmacophore model

Pharmacophore feature data provides critical information about the spatial arrangement of functional groups or chemical moieties that are essential for a molecule to bind to its target receptor and elicit a biological response (Gao et al., 2017). In this article, we have a pharmacophore model that has been evaluated using pairwise alignments, which is a common method used to compare the similarity between two molecules based on their chemical features. The best pairwise alignment of the pharmacophore model has a score of 15.0452, which indicates a good degree of similarity between the two molecules being compared (Table 1). This score can be used to rank different alignment models and select the most appropriate one for further analysis.

The pharmacophore model was characterized by nine features, including one aromatic, three hydrogen donors, and five hydrogen acceptors. A report that ligand-based virtual screening identifies SARS-CoV-2 3CLpro inhibitors using nine features, including one aromatic, three hydrogen donors, and five hydrogen acceptors (Glaab et al., 2021), where these features are critical for binding to the target receptor and are essential for the biological activity of the molecule. The spatial arrangement of these features is also important, as it determines how well the molecule can interact with the receptor and trigger a response. The six spatial features in the pharmacophore model indicate that the molecule has a relatively complex structure and is likely to have a high degree of specificity for its target receptor. This is because the more features a molecule has, the more specific it can be in terms of its binding interactions with the receptor.

Overall, the pharmacophore feature data provided here is a valuable tool for understanding the molecular interactions that underlie the biological activity of a molecule. By identifying the key features and their spatial arrangement, new molecules that were optimized for binding to a specific receptor and eliciting a desired biological response.

Validation pharmacophore model

The validation of the pharmacophore model is critical in pharmacophore-based drug development to verify that the model can reliably identify active molecules and separate them from inactive ones (Hammad et al., 2020). The ROC curve, which analyzes the model's capacity to distinguish between active and inactive substances, is one of the most often used validation metrics. The ROC plots the true positive rate

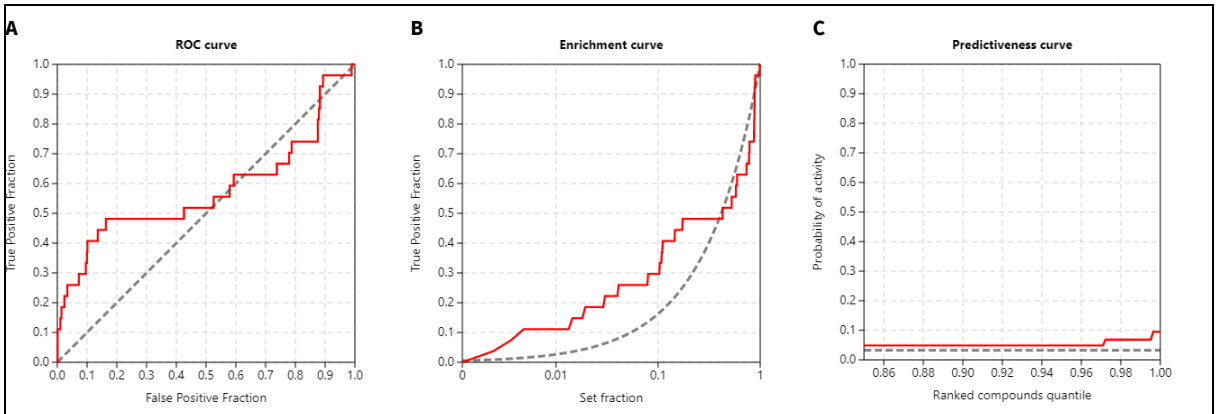

Figure 1. Parameter for validation pharmacophore model.
(A) ROC_curves, **(B)** Enrichment_curves, and **(C)** Predictiveness_curves.

(TPR) *vs*. the false positive rate (FPR) for various threshold values (Kaserer et al., 2015). The ROC curve in this scenario was created utilizing a dataset of 828 decoys and 27 active compounds, allowing the identification of 801 inactive compounds. The hit rate, or percentage of active compounds identified by the model, was 3.26 percent, showing that the model was only moderately successful in identifying active chemicals (Fig. 1).

The greatest reachable enrichment factor (EF), which quantifies the model's capacity to detect active chemicals more efficiently than random screening, is another significant validation parameter. The maximum achievable EF was determined to be 30.67, indicating that the approach may be beneficial in identifying active chemicals with substantially better efficiency than random screening.

The AUC number is a measure of the model's overall performance, with a greater value indicating better performance. In this situation, the AUC value of 0.576 indicates that the pharmacophore model has a moderate ability to distinguish between active and inactive drugs. Total gain (TG) is another statistic that quantifies the improvement in enrichment over a random selection of chemicals. It is calculated as the ratio of the number of active compounds recovered by the model to the total number of compounds screened. The TG value of 0.144 suggests that the pharmacophore model has a modest enrichment over random selection. Relative information content (RIE) is a metric that assesses the model's discrimination power in ranking active compounds higher than inactive ones. It is determined as the ratio of the difference between the average ranks of active and inactive compounds to the total number of compounds screened. The RIE value of 4.379 indicates that the pharmacophore model is relatively good at ranking active chemicals higher than inactive ones.

Binary ensemble averaged ROC (BEDROC) is a statistic that considers the enrichment of the top-ranked compounds. It is calculated as the weighted average of the ROC curve, with the weights based on the rank of the compounds. The BEDROC value of 0.298 suggests that the pharmacophore model has a moderate enrichment of the top-ranked drugs.

In the context of pharmacophore modeling, the number of active and inactive compounds used for validation can vary. Some studies mentioned in the search results used a set of 10 active compounds and thousands of inactive compounds for validation (Opo et al., 2021). Other studies utilized a set of previously known inhibitors or a diverse set of active compounds for validation (Aman et al., 2021). The specific number of compounds used for validation may depend on the availability of experimental data or the size of the compound library being screened.

Finally, the average rank of actives is a metric that quantifies the model's ranking performance for active compounds. The model performs better when the average rank was lower. In this situation, the average rank of actives was 353.93, showing that the pharmacophore model was moderately good at ranking active molecules.

Screening performance

The hits and free energy of binding (Table 2) indicate that the pharmacophore model can identify active compounds from a broad pool of molecules. The virtual screening of 270,547 natural product library molecules yielded 75 hits, demonstrating the model's ability to find prospective medication candidates. The discovery of test ligands with considerably lower free energy of binding than the reference natural ligand suggests that the model has the potential to identify compounds with higher binding affinities, which is an important factor in drug discovery.

Table 2. Training set (Tong et al., 2022) and best pairwise solution of a pharmacophore model.

Zinc IDS	Free energy of binding, ΔG (kcal/mol)	Zinc IDS	Free energy of binding, ΔG (kcal/mol)	Zinc IDS	Free energy of binding, ΔG (kcal/mol)
ZINC000085567870	-10.95	ZINC000097971976	-7.63	ZINC000096221638	-6.42
ZINC000085567845	-9.54	ZINC000095485922	-7.47	ZINC000150653691	-6.42
ZINC000095485991	-9.36	ZINC000006523948	-7.42	ZINC000014437211	-6.38
ZINC000085567854	-9.24	ZINC000108451402	-7.42	ZINC000033832193	-6.38
ZINC000085567860	-9.2	ZINC000108449334	-7.41	ZINC000020464710	-6.37
ZINC000085567851	-9.05	ZINC000096222811	-7.29	ZINC000150653434	-6.37
ZINC000085567875	-8.96	ZINC000014639742	-7.28	ZINC000016215132	-6.35
ZINC000085739881	-8.83	ZINC000108447625	-7.24	ZINC000150653025	-6.34
ZINC000013312346	-8.73	ZINC000084713616	-7.23	ZINC000014760969	-6.33
ZINC000085739890	-8.69	ZINC000085567814	-7.23	ZINC000096114465	-6.32
ZINC000096113763	-8.65	ZINC000013379920	-7.19	ZINC000097972043	-6.22
ZINC000085567837	-8.56	ZINC000084713617	-7.0	ZINC000108448225	-6.22
ZINC000015256039	-8.55	ZINC000095910001	-6.88	ZINC000096116260	-6.21
ZINC000085567855	-8.54	ZINC000096115118	-6.86	ZINC000150652972	-6.13
ZINC000084713610	-8.44	ZINC000097971931	-6.85	ZINC000108448157	-6.09
ZINC000108449284	-8.21	ZINC000096115865	-6.84	ZINC000150653023	-6.07
ZINC000097971975	-7.97	ZINC000097972037	-6.84	ZINC000150652971	-6.01
ZINC000096115864	-7.95	ZINC000108449897	-6.83	ZINC000150653269	-6.01
ZINC000013412027	-7.89	ZINC000002556383	-6.81	ZINC000096115205	-5.95
ZINC000096115435	-7.87	ZINC000014640449	-6.63	ZINC000108448257	-5.86
ZINC000095099479	-7.86	ZINC000014762765	-6.59	ZINC000096114853	-5.77
ZINC000015120655	-7.8	ZINC000096114091	-6.5	ZINC000096115328	-5.72
ZINC000097972044	-7.79	ZINC000014436868	-6.49	ZINC000150653689	-5.58
ZINC000108451395	-7.7	ZINC000096116261	-6.48	ZINC000108451190	-5.57
ZINC000604404440	-7.66	ZINC000096115682	-6.43	Native ligand	-5.36

Overall, the hits and free energy of binding statistics show the pharmacophore model's capacity for discovering active compounds from a broad pool of compounds and highlight its utility as a tool in the drug discovery process. The free energy of binding is an important metric for determining ligand binding affinity to a protein target. In this scenario, three distinct molecules were docked into the binding site of the 7BQY protein: the native ligand, ZINC 000085567870, and ZINC000085567845. The native ligand has a binding free energy of -5.36 kcal/mol, whereas ZINC000085567870 and ZINC000085567845 have binding free energies of -10.95 kcal/mol and -9.54 kcal/mol, respectively. When the free energy of binding values was compared, we can find that ZINC000085567870 and ZINC000085567845 have higher binding affinities to the 7BQY protein than the natural ligand. ZINC000085567870 has the highest free energy of binding value, indicating that it is the most effective of the three compounds.

PDB structures such as 7BQY, 6LU7, 6W63, 7C7P, and 7JU7 are commonly used for virtual screening of SARS-CoV-2 main protease inhibitors. Between receptors' respective docking, the highest correlation coefficient is 0.85 for 7BQY (Clyde et al., 2021). Docking data feature analysis is a novel approach to evaluating virtual screening experiments based on the analysis of docking output data (Arciniega and Lange, 2014).

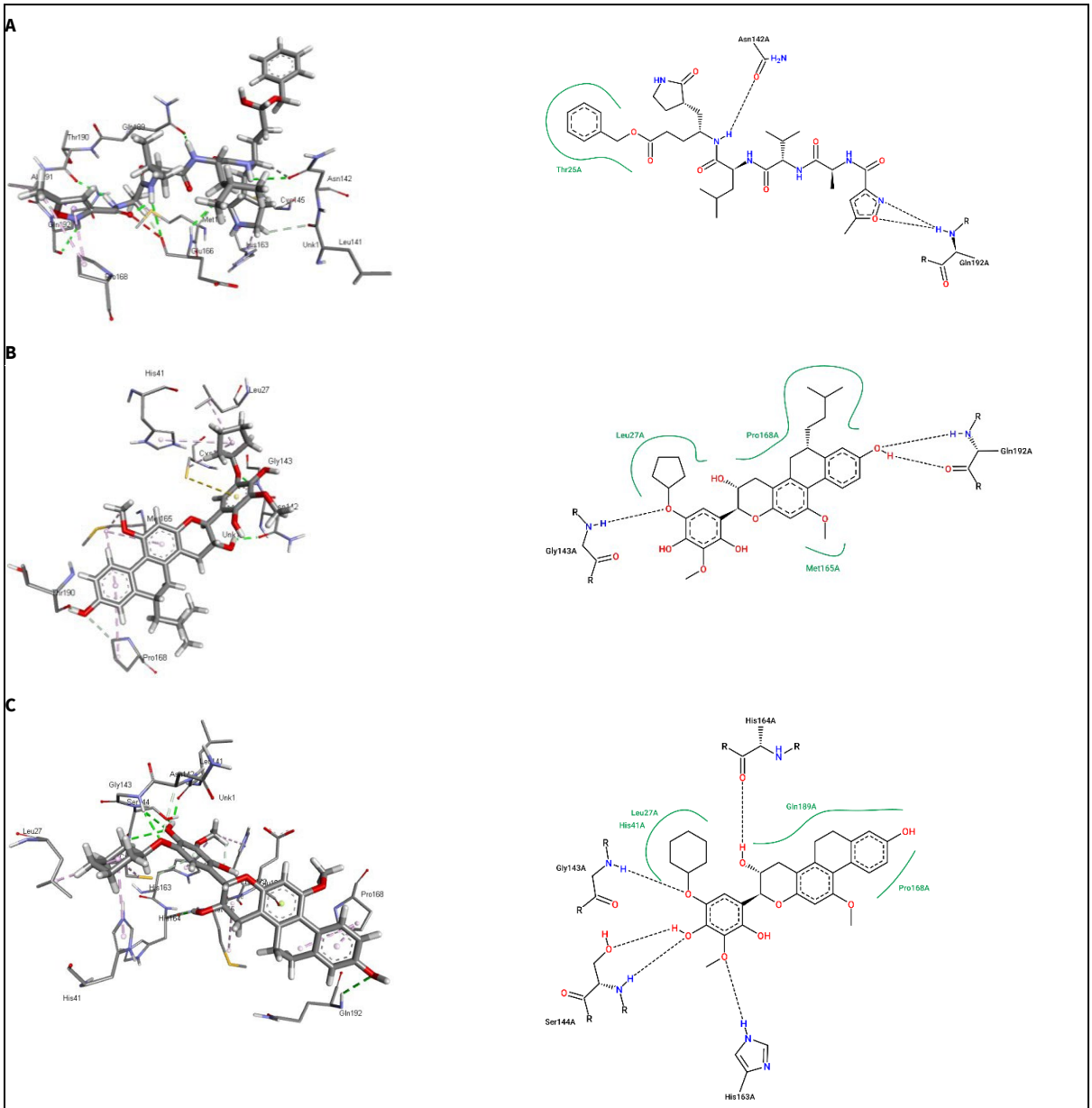

Figure 2. 2D and 3D representation of the top two hits with interaction on the active site (PDB ID 7BQY).
(A) Native ligand, **(B)** ZINC000085567870, and **(C)** ZINC000085567845.

Molecular interactions of the best ligands

To build successful drugs, it is critical to understand the interactions between ligands and their target proteins during the drug discovery process (Higueruelo et al., 2013). The interaction data for the native ligand into the 7BQY binding site provides insight into the ligand's binding mechanism and the major interactions involved (Fig. 2A). The native ligand makes five hydrogen bonds with the amino acid residues ASN142, GLN189, GLU166, THR190, and GLN192, according to the data. Hydrogen bonds are critical in protein-ligand interactions because they give the binding complex specificity and stability. Multiple hydrogen bonds formed with distinct amino acid residues indicate that the ligand is well accommodated within the binding pocket and has a high affinity for the target protein. The native ligand forms six Pi-alkyl interactions with amino acid residues HIS163, CYS145, MET165, PRO168, and ALA191 in addition to hydrogen bonds. A planar aromatic ring in the ligand interacts with the hydrophobic side chains of amino acid residues in the protein to form pi-alkyl interactions. By generating extra van der Waals contacts, these interactions help to stabilize the protein-ligand complex.

The interaction data for ZINC000085567870 in the 7BQY binding site gives insight into the ligand's binding mechanism and the essential interactions involved (Fig. 2B). ZINC000085567870 generates seven hydrogen bonds with amino acid residues HS164, GLN192,

CYS145, LEU141, GLY143, and SER144, according to the data. These hydrogen bonds contribute to the protein-ligand complex's specificity and stability. Multiple hydrogen bonds formed with distinct amino acid residues suggest that the ligand is well-accommodated within the binding pocket and has a high affinity for the target protein. ZINC000085567870 generates seven Pi-alkyl connections with amino acid residues PRO168, MET165, HIS172, HIS163, HIS41, LEU27, and hydrogen bonds. These Pi-alkyl interactions take place between the ligand's planar aromatic ring and the hydrophobic side chains of amino acid residues in the protein. These interactions contribute to the protein-ligand complex's stability by providing additional van der Waals connections.

The interaction data for ZINC000085567845 into the binding site of 7BQY reveals the ligand's binding mechanism as well as the essential interactions involved in the creation of the protein-ligand complex. ZINC000085567845 makes three hydrogen bonds with the amino acid residues ASN142, GLY143, and THR190, according to the data. By generating favorable electrostatic contacts between the ligand and protein, these hydrogen bonds contribute to the specificity and stability of the protein-ligand complex. Furthermore, ZINC000085567845 establishes seven Pi-alkyl connections with PRO168, MET165, CYS145, HIS41, and LEU27 amino acid residues. The Pi-alkyl interactions occur between the ligand's planar aromatic ring and the hydrophobic side chains of the protein's amino acid residues. These interactions contribute to the protein-ligand complex's stability by providing additional van der Waals connections.

The interaction data for ZINC000085567845 in the 7BQY binding site indicate that the ligand interacts with the protein with moderate specificity and affinity (Fig. 2C). The establishment of hydrogen bonds and Pi-alkyl interactions suggests that the ligand interacts with important amino acid residues in the protein, which contributes to the complex's stability. Despite forming fewer hydrogen bonds than ZINC000085567870, the ligand nevertheless interacts with key amino acid residues in the binding pocket.

Based on the analysis of the docking results for SARS-CoV-2 main protease 3CLpro (7BQY), hydrogen bonds and some non-classical hydrogen bonds could be observed for the chloroquine binding process. The hydrogen bond was generated with residue Cys145 at a distance of 2.67 Å, while the aliphatic chain was in carbon-hydrogen bond contact with His163, Glu166, Phe140, and Asn142. Mefloquine is involved in hydrogen bond interactions with Cys145 and Asn1421 (EL Khatabi et al., 2022).

Stability interactions of the best ligands

Molecular dynamics analysis is a computational method used to study the behavior of molecules over time. It involves simulating the motion of atoms and molecules in a system and analyzing the resulting data. RMSD is a measure of the difference between the positions of atoms in two structures, while RMSF is a measure of the flexibility of a molecule. Energy components data refers to the different types of energy that contribute to the stability of a molecule, such as electrostatic, van der Waals, and solvation energies. Molecular dynamics analysis has been used to study the dynamics of the ACE2-SARS-CoV-2/SARS-CoV spike protein (Ali and Vijayan, 2020), the molecular interactions between the SARS-CoV-2 spike protein and ACE2 (Martí et al., 2022), and the impact of spike protein mutations on virus transmission (Chen et al., 2022). It has also been used to identify novel unbound substates of the SARS-CoV-2 spike protein that may represent new targets for therapeutic design (Williams et al., 2022). Molecular dynamics analysis can provide valuable insights into the behavior of molecules and their interactions and can aid in the development of new drugs and therapies.

RMSD

The RMSD values indicate the deviation or displacement of the molecules' structures from their initial conformations. Analyzing the data, at the beginning of the simulation, all three molecules have an RMSD of 0, indicating that their structures closely resemble their initial conformations. Overall RMSD trends show that NL ((E,4S)-4-azanyl-5-[(3S)-2-oxidanylidenepyrrolidin-3-yl]pent-2enoic acid) displays a relatively higher RMSD compared to the other two molecules throughout the simulation. This suggests that NL undergoes larger structural deviations or fluctuations over the 100 ns timeframe (Fig. 3). ZINC000085567845 and ZINC000085567870 generally exhibit lower RMSD values compared to NL, indicating relatively smaller structural changes or more stable conformations.

Specific time points showed that at time points 2 ns, 5 ns, 7 ns, and 10 ns, NL consistently shows higher RMSD values than the other two molecules. This suggests that NL experiences more significant structural deviations at these time points. At time points 63 ns, 85 ns, and 100 ns, NL continues to exhibit a higher RMSD compared to ZINC000085567845 and ZINC000085567870. However, the RMSD values for all three molecules decrease over time, suggesting some convergence towards more stable conformations. These observations indicate that NL generally undergoes larger structural fluctuations or deviations compared to ZINC000085567845 and

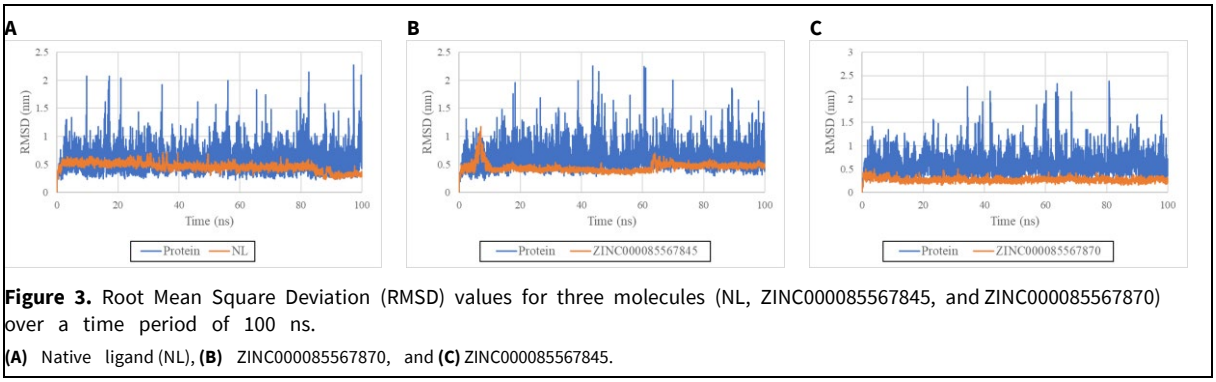

Figure 3. Root Mean Square Deviation (RMSD) values for three molecules (NL, ZINC000085567845, and ZINC000085567870) over a time period of 100 ns.
(A) Native ligand (NL), **(B)** ZINC000085567870, and **(C)** ZINC000085567845.

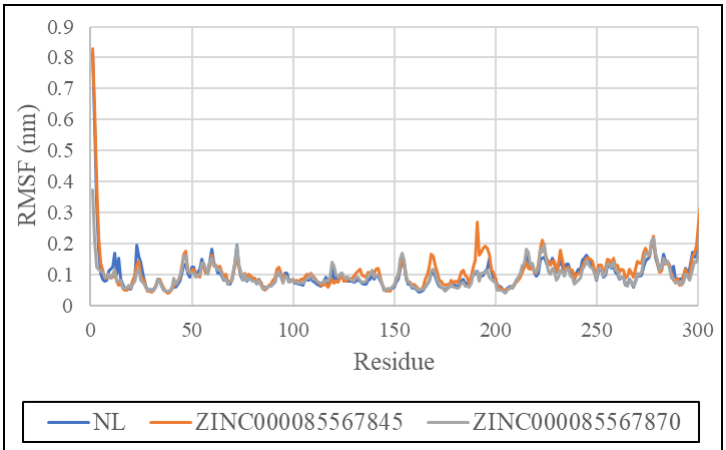

Figure 4. Root-mean-square fluctuation (RMSF) data were obtained for specific residues in a protein structure.

ZINC000085567870 over the simulated 100 ns timeframe. The lower RMSD values observed for ZINC000085567845 and ZINC000085567870 suggest that these molecules exhibit relatively more stable conformations or smaller structural changes.

The results are consistent with the summary from the journal article by EL Khatabi et al. (2022), which shows that the molecular dynamics simulation had RMSD fluctuations around 0.2–0.3 Å with small conformational changes of the protein-ligand complex.

RMSF

The RMSF is a measure of the flexibility and mobility of protein residues in molecular dynamics simulations. In this discussion, we compare the RMSF profiles of three different entities: NL, ZINC000085567845, and ZINC000085567870. These entities represent distinct molecules or conformations under investigation. By examining their RMSF profiles, we can gain insights into their structural dynamics and identify regions of high flexibility.

The overall RMSF range (Fig. 4), at a residue of 23, showed that NL has the highest RMSF value of 0.1936, indicating higher flexibility compared to ZINC000085567845 (0.1348) and ZINC000085567870 (0.1079). This suggests that NL experiences more fluctuations and potentially exhibits greater conformational changes in this region. A residue of 47 shows that, once again, NL has the highest RMSF value (0.1349), followed by ZINC000085567845 (0.1748) and ZINC000085567870 (0.1617). Similar to residue 23, NL shows higher flexibility, indicating potential conformational changes. For residue 60, NL (0.1818) exhibits the highest RMSF, followed by ZINC000085567845 (0.1624) and ZINC000085567870 (0.1531). This suggests that NL may have greater flexibility in this region, possibly indicating a dynamic structural feature or interaction. For residue 72, NL (0.1939) once again demonstrates the highest RMSF value, indicating increased flexibility compared to ZINC000085567845 (0.1497) and ZINC000085567870 (0.1909). This suggests that residue 72 in NL may have a higher propensity for conformational changes. For residue 155, NL exhibits the highest RMSF value (0.1339) for residue 155, followed by ZINC000085567845 (0.1354) and ZINC000085567870 (0.1463). The similar values suggest that these molecules experience comparable flexibility at this residue. For residue 169, NL (0.1082) and ZINC000085567845 (0.1579) show higher RMSF val-

ues compared to ZINC000085567870 (0.1163) for residue 169. This indicates that NL and ZINC 000085567845 experience greater flexibility, while ZINC000085567870 exhibits relatively lower flexibility at this residue. For residue 191, NL (0.1336) and ZINC000085567870 (0.1031) demonstrate higher RMSF values compared to ZINC000085567845 (0.0966) for residue 191. This suggests that NL and ZINC000085567870 have higher flexibility, potentially indicating conformational changes or interactions. For residue 197, NL (0.1011) shows the highest RMSF value for residue 197, followed by ZINC000085567845 (0.0769) and ZINC000085567870 (0.0782). This indicates that NL has higher flexibility, while the other two molecules exhibit relatively lower fluctuations. For residue 277, NL (0.1107) demonstrates the highest RMSF value, followed by ZINC000085567845 (0.116) and ZINC000085567870 (0.1134). These values indicate that all three molecules experience similar flexibility in this region. Overall, NL tends to exhibit higher RMSF values, suggesting greater flexibility and potential conformational changes compared to the other two molecules, ZINC000085567845 and ZINC 000085567870. These differences in flexibility could be attributed to variations in molecular structure, interactions, or binding events specific to NL.

The results are consistent with the summary from the journal article by EL Khatabi et al. (2022), which shows that the molecular dynamics simulation had RMSF fluctuations less than 0.3 Å with small conformational changes of the amino acid residues.

Energy components

The ΔEVDWAALS component represents the Van der Waals interactions, which play a crucial role in ligand binding. All three compounds exhibit negative values, indicating favorable Van der Waals interactions with their respective targets (Fig. 5). The ΔEEL component reflects the electrostatic interactions. Again, all three compounds have negative values, indicating favorable electrostatic interactions and stability within their binding sites. ΔEGB represents the generalized born electrostatic solvation energy. Positive values suggest that the compounds are less favorable in the solvent environment, whereas negative values indicate more favorable solvation states. In this case, all three compounds have negative values, suggesting that they are well-suited to the solvent environment and may experience favorable solvation effects. ΔESURF accounts for the change in nonpolar solvation energy, which relates to hydrophobic interactions. Negative values imply favorable hydrophobic interactions, indicating good compatibility with the target binding site. Once again, all three compounds exhibit negative values, suggesting optimized nonpolar solvation energies and potential hydrophobic interactions with their targets. ΔGGAS represents the gas-phase free energy change. Negative values suggest that the compounds are more stable in the gas phase, indicating favorable interactions. All three compounds have negative ΔGGAS values, implying their inherent stability and potential for efficient binding. ΔGSOLV accounts for the solvation-free energy change. Positive values indicate that the compounds are less stable upon solvation, whereas negative values suggest solvation stabilization. All three compounds have negative ΔGSOLV values, indicating their favorable solvation properties and stability in the solvent environment. Finally, ΔETOTAL represents the overall energy change of the system upon ligand binding. All three compounds have negative ΔETOTAL values, indicating that their binding is energetically favorable. This suggests that NL, ZINC000085567845, and ZINC000085567870 have strong affinities for their respective targets and favorable interaction profiles.

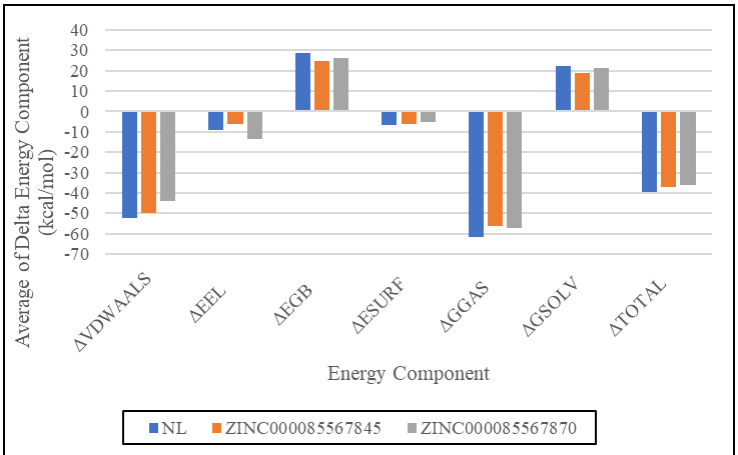

Figure 5. Energy Components of a protein-ligand complex for native ligand (NL), ZINC000085567870, and ZINC000085567845.

In summary, all three compounds exhibit energy components that are consistent with favorable ligand binding. The negative values of ΔVDWAALS and ΔEEL indicate optimized Van der Waals and electrostatic interactions, respectively, suggesting good complementarity with the target binding sites. Additionally, the negative ΔESURF values suggest favorable hydrophobic interactions, while the negative ΔGSOLV values indicate stability in the solvent environment. Furthermore, the negative ΔGGAS values and negative ΔTOTAL values reflect the overall favorable energy changes upon ligand binding. Despite these energetic changes, the energy of these systems remained negative, indicating that the complexes continued to demonstrate excellent stability. This is consistent with what Hayek-Orduz et al. (2022) reported.

CONCLUSION

Six small-molecule metabolites from human blood were examined for their potential to screen a natural product database for the SARS-CoV-2 spike protein inhibitor. The AUC value of the pharmacophore model generated using the best pairwise alignments strategy was 0.576, indicating that it has been adequately validated as a model. Using the pharmacophore model for virtual screening, followed by molecular docking, 75 hits were discovered. The molecular dynamics analysis of two top-rank hits (ZINC000085567845 and ZINC000085567870) indicated a stable interaction with the SARS-CoV-2 spike protein. The created pharmacophore model was able to generate lead compounds with the potential to inhibit the SARS-CoV-2 spike protein.

CONFLICT OF INTEREST

The authors declare no conflicts of interest.

ACKNOWLEDGMENTS

This research did not receive any specific grant from funding agencies in the public, commercial, or not-for-profit sectors.

REFERENCES

Adrià CM, Garcia-Vallvé S, Pujadas G (2012) DecoyFinder, a tool for finding decoy molecules. J Cheminform 4(suppl. 1): P2. https://doi.org/10.1186/1758-2946-4-S1-P2

Ali A, Vijayan R (2020) Dynamics of the ACE2–SARS-CoV-2/SARS-CoV spike protein interface reveal unique mechanisms. Sci Rep 10: 14214. https://doi.org/10.1038/s41598-020-71188-3

Aman LO, Kartasasmita RE, Tjahjono DH (2021) Virtual screening of curcumin analogues as DYRK2 inhibitor: Pharmacophore analysis, molecular docking and dynamics, and ADME prediction. F1000Research 10: 394. https://doi.org/10.12688/f1000research.28040.1

Arciniega M, Lange OF (2014) Improvement of virtual screening results by docking data feature analysis. J Chem Inf Model 54: 1401–1411. https://doi.org/10.1021/ci500028u

Asnawi A, Nedja M, Febrina E, Purwaniati P (2023) Prediction of a stable complex of compounds in the ethanol extract of celery leaves (*Apium graveolens* L.) function as a VKORC1 antagonist. Trop J Nat Prod Res 7: 2362–2370 http://www.doi.org/10.26538/tjnpr/v7i2.10

Bernardi A, Faller R, Reith D, Kirschner KN (2019) ACPYPE update for nonuniform 1–4 scale factors: Conversion of the GLYCAM06 force field from AMBER to GROMACS. SoftwareX 10: 100241. https://doi.org/10.1016/j.softx.2019.100241

Case DA, Aktulga HM, Belfon K, Ben-Shalom IY, Brozell SR, Cerutti DS, Cheatham III TE, Cisneros GA, Cruzeiro VWD, Darden TA, Duke RE, Giambasu G, Gilson MK, Gohlke H, Goetz AW, Harris R, Izadi S, Izmailov SA, Jin C, Kasavajhala K, Kaymak MC, King E, Kovalenko A, Kurtzman T, Lee TS, LeGrand S, Li P, Lin C, Liu J, Luchko T, Luo R, Machado M, Man V, Manathunga M, Merz KM, Miao Y, Mikhailovskii O, Monard G, Nguyen H, O'Hearn KA, Onufriev A, Pan F, Pantano S, Qi R, Rahnamoun A, Roe DR, Roitberg A, Sagui C, Schott-Verdugo S, Shen J, Simmerling CL, Skrynnikov NR, Smith J, Swails J, Walker RC, Wang J, Wei H, Wolf RM, Wu X, Xue Y, York DM, Zhao S, Kollman PA (2021) Amber 2021, University of California, San Francisco.

Chen P, Wang J, Xu X, Li Y, Zhu Y, Li X, Li M, Hao P (2022) Molecular dynamic simulation analysis of SARS-CoV-2 spike mutations and evaluation of ACE2 from pets and wild animals for infection risk. Comput Biol Chem 96: 107613. https://doi.org/10.1016/j.compbiolchem.2021.107613

Citarella A, Scala A, Piperno A, Micale N (2021) SARS-CoV-2 M^{pro}: A potential target for peptidomimetics and small-molecule inhibitors. Biomolecules 11: 607. https://doi.org/10.3390/biom11040607

Clyde A, Galanie S, Kneller DW, Ma H, Babuji Y, Blaiszik B, Brace A, Brettin T, Chard K, Chard R, Coates L, Foster I, Hauner D, Kertesz V, Kumar N, Lee H, Li Z, Merzky A, Schmidt JG, Tan L, Titov M, Trifan A, Turilli M, Van Dam H, Chennubhotla SC, Jha S, Kovalevsky A, Ramanathan A, Head MS, Stevens R (2021) High-throughput virtual screening and validation of a SARS-CoV-2 main protease noncovalent inhibitor. J Chem Inf Model 62(1): 116–128. https://doi.org/10.1021/acs.jcim.1c00851

Dallakyan S, Olson AJ (2015) Small-molecule library screening by docking with PyRx. Methods Mol Biol 1263: 243-250. https://doi.org/10.1007/978-1-4939-2269-7_19

EL Khatabi K, Aanouz I, Alaqarbeh M, Ajana MA, Lakhlifi T, Bouachrine M (2022) Molecular docking, molecular dynamics simulation, and ADMET analysis of levamisole derivatives against the SARS-CoV-2 main protease (M^{Pro}). Bioimpacts 12: 107–113. https://doi.org/10.34172/bi.2021.22143

El-Ashrey MK, Bakr RO, Fayed MAA, Refaey RH, Nissan YM (2022) Pharmacophore based virtual screening for natural product database revealed possible inhibitors for SARS-COV-2 main protease. Virology 570: 18–28. https://doi.org/10.1016/j.virol.2022.03.003

Empereur-Mot C, Zagury J-F, Montes M (2016) Screening explorer–An interactive tool for the analysis of screening results. J Chem Inf Model 56: 2281–2286. https://doi.org/10.1021/acs.jcim.6b00283

Febrina E, Asnawi A, Abdulah R, Lestari K, Supratman U (2022) Identification of flavonoids from *Acalypha indica* L. (Euphorbiaceae) as caspase-3 activators using molecular docking and molecular dynamics. Int J Appl Pharm 14: 162–166. https://doi.org/10.22159/ijap.2022.v14s5.34

Gao Q, Wang Y, Hou J, Yao Q, Zhang J (2017) Multiple receptor-ligand based pharmacophore modeling and molecular docking to screen the selective inhibitors of matrix metalloproteinase-9 from natural products. J Comput Aided Mol Des 31: 625–641. https://doi.org/10.1007/s10822-017-0028-3

Gaulton A, Hersey A, Nowotka M, Bento AP, Chambers J, Mendez D, Mutowo P, Atkinson F, Bellis LJ, Cibrián-Uhalte E, Davies M, Dedman N, Karlsson A, Magariños MP, Overington JP, Papadatos G, Smit I, Leach AR (2017) The ChEMBL database in 2017. Nucleic Acids Res 45: D945–D954. https://doi.org/10.1093/nar/gkw1074

Genheden S, Ryde U (2015) The MM/PBSA and MM/GBSA methods to estimate ligand-binding affinities. Expert Opin Drug Discov 10: 449–461. https://doi.org/10.1517/17460441.2015.1032936

Glaab E, Manoharan GB, Abankwa D (2021) Pharmacophore model for SARS-CoV-2 3CLpro small-molecule inhibitors and *in vitro* experimental validation of computationally screened inhibitors. J Chem Inf Model 61: 4082–4096. https://doi.org/10.1021/acs.jcim.1c00258

Hammad S, Bouaziz-Terrachet S, Meghnem R, Meziane D (2020) Pharmacophore development, drug-likeness analysis, molecular docking, and molecular dynamics simulations for identification of new CK2 inhibitors. J Mol Model 26: 160. https://doi.org/10.1007/s00894-020-04408-2

Hayek-Orduz Y, Vásquez AF, Villegas-Torres MF, Caicedo PA, Achenie LEK, González Barrios AF (2022) Novel covalent and non-covalent complex-based pharmacophore models of SARS-CoV-2 main protease (M^{pro}) elucidated by microsecond MD simulations. Sci Rep 12: 14030. https://doi.org/10.1038/s41598-022-17204-0

He X, Man VH, Yang W, Lee TS, Wang J (2020) A fast and high-quality charge model for the next generation general AMBER force field. J Chem Phys 153: 114502. https://doi.org/10.1063/5.0019056

Higueruelo AP, Jubb H, Blundell TL (2013) Protein-protein interactions as druggable targets: Recent technological advances. Curr Opin Pharmacol 13: 791–796. https://doi.org/10.1016/j.coph.2013.05.009

Huey R, Morris GM, Forli S (2012) Using AutoDock 4 and AutoDock vina with AutoDockTools: A tutorial. The Scripps Research Institute Molecular Graphics Laboratory, pp. 46.

Jackson CB, Farzan M, Chen B, Choe H (2022) Mechanisms of SARS-CoV-2 entry into cells. Nat Rev Mol Cell Biol 23: 3–20. https://doi.org/10.1038/s41580-021-00418-x

Jejurikar BL, Rohane SH (2021) Drug designing in discovery studio. Asian J Res Chem 14: 135-138. https://doi.org/10.5958/0974-4150.2021.00025.0

Kaserer T, Beck KR, Akram M, Odermatt A, Schuster D (2015) Pharmacophore models and pharmacophore-based virtual screening: Concepts and applications exemplified on hydroxysteroid dehydrogenases. Molecules 20: 22799–22832. https://doi.org/10.3390/molecules201219880

Kim S, Chen J, Cheng T, Gindulyte A, He J, He S, Li Q, Shoemaker BA, Thiessen PA, Yu B, Zaslavsky L, Zhang J, Bolton EE (2019) PubChem 2019 update: Improved access to chemical data. Nucleic Acids Res 47: D1102–D1109. https://doi.org/10.1093/nar/gky1033

Krammer F (2020) SARS-CoV-2 vaccines in development. Nature 586(7830): 516–527. https://doi.org/10.1038/s41586-020-2798-3

Kutzner C, Kniep C, Cherian A, Nordstrom L, Grubmüller H, de Groot BL, Gapsys V (2022) GROMACS in the cloud: A global supercomputer to speed up alchemical drug design. J Chem Inf Model 62: 1691–1711. https://doi.org/10.1021/acs.jcim.2c00044

La Torre F, Leonardi L, Giardino G, Volpi S, Federici S, Soresina A, Cancrini C, Lougaris V, Castagnoli R, Corrente S, Cardinale F; Immunology Commission of the Italian Society of Pediatric Allergy, Immunology (SIAIP) (2020) Immunological basis of virus-host interaction in COVID-19. Pediatr Allergy Immunol 31 (Suppl. 26): 75–78. https://doi.org/10.1111/pai.13363

Li G, De Clercq E (2020) Therapeutic options for the 2019 novel coronavirus (2019-nCoV). Nat Rev Drug Discov 19: 149–150. https://doi.org/10.1038/d41573-020-00016-0

Liu P, Liu H, Sun Q, Liang H, Li C, Deng X, Liu Y, Lai L (2020) Potent inhibitors of SARS-CoV-2 3C-like protease derived from N-substituted isatin compounds. Eur J Med Chem 206: 112702. https://doi.org/10.1016/j.ejmech.2020.112702

Mark P, Nilsson L (2001) Structure and dynamics of the TIP3P, SPC, and SPC/E water models at 298 K. J Phys Chem A 105: 9954–9960. https://doi.org/10.1021/jp003020w

Martí D, Alsina M, Alemán C Bertran O, Turon P, Torras J (2022) Unravelling the molecular interactions between the SARS-CoV-2 RBD spike protein and various specific monoclonal antibodies. Biochimie 193: 90–102. https://doi.org/10.1016/j.biochi.2021.10.013

Mayer KA, Stöckl J, Zlabinger GJ, Gualdoni GA (2019) Hijacking the supplies: Metabolism as a novel facet of virus-host interaction. Front Immunol 10: 1533. https://doi.org/10.3389/fimmu.2019.01533

Ndwandwe D, Wiysonge CS (2021) COVID-19 vaccines. Curr Opin Immunol 71: 111–116. https://doi.org/10.1016/j.coi.2021.07.003

Opo FADM, Rahman MM, Ahammad F, Ahmed I, Bhuiyan MA, Asiri AM (2021) Structure based pharmacophore modeling, virtual screening, molecular docking and ADMET approaches for identification of natural anti-cancer agents targeting XIAP protein. Sci Rep 11: 4049. https://doi.org/10.1038/s41598-021-83626-x

Ritchie TJ, McLay IM (2012) Should medicinal chemists do molecular modelling? Drug Discov Today 17: 534–537. https://doi.org/10.1016/j.drudis.2012.01.005

Schneidman-Duhovny D, Dror O, Inbar Y, Nussinov R, Wolfson HJ (2008) PharmaGist: a webserver for ligand-based pharmacophore detection. Nucleic Acids Res 36: W223–W228. https://doi.org/10.1093/nar/gkn187

Sterling T, Irwin JJ (2015) ZINC 15–ligand discovery for everyone. J Chem Inf Model 55: 2324–2337. https://doi.org/10.1021/acs.jcim.5b00559

Tong L, Xiao X, Li M, Fang S, Ma E, Yu X, Zhu Y, Wu C, Tian D, Yang F, Sun J, Qu J, Zheng N, Liao S, Tai W, Feng S, Zhang L, Li Y, Wang L, Han X, Sun S, Yang L, Zhong H, Zhao J, Liu W, Liu X, Wang P, Li L, Zhao G, Zhang R, Cheng G (2022) A glucose-like metabolite deficient in diabetes inhibits cellular entry of SARS-CoV-2. Nat Metab 4: 547–558. https://doi.org/10.1038/s42255-022-00567-z

Williams JK, Wang B, Sam A, Hoop CL, Case DA, Baum J (2022) Molecular dynamics analysis of a flexible loop at the binding interface of the SARS-CoV-2 spike protein receptor-binding domain. Proteins 90: 1044–1053. https://doi.org/10.1002/prot.26208

Zhou P, Yang X-L, Wang X-G, Hu B, Zhang L, Zhang W, Si HR, Zhu Y, Li B, Huang CL, Chen HD, Chen J, Luo Y, Guo H, Jiang RD, Liu MQ, Chen Y, Shen XR, Wang X, Zheng XS, Zhao K, Chen QJ, Deng F, Liu LL, Yan B, Zhan FX, Wang YY, Xiao GF, Shi ZL (2020) A pneumonia outbreak associated with a new coronavirus of probable bat origin. Nature 579: 270–273. https://doi.org/10.1038/s41586-020-2012-7

AUTHOR CONTRIBUTION:

Contribution	Febrina E	Asnawi A
Concepts or ideas	x	
Design	x	x
Definition of intellectual content	x	x
Literature search	x	x
Experimental studies	x	x
Data acquisition	x	x
Data analysis	x	x
Statistical analysis	x	x
Manuscript preparation	x	x
Manuscript editing	x	x
Manuscript review	x	x

Citation Format: Febrina E, Asnawi A (2023) Lead compound discovery using pharmacophore-based models of small-molecule metabolites from human blood as inhibitor cellular entry of SARS-CoV-2. J Pharm Pharmacogn Res 11(5): 810–822. https://doi.org/10.56499/jppres23.1688_11.5.810